Mineralium Deposita (2003) 38: 141–153
DOI 10.1007/s00126-002-0290-7

ARTICLE

Xiao'ou Zhang · Peter A. Cawood · Simon A. Wilde
Ruqi Liu · Hailin Song · Wen Li · Lawrence W. Snee

Geology and timing of mineralization at the Cangshang gold deposit, north-western Jiaodong Peninsula, China

Received: 2 November 1999 / Accepted: 12 March 2002 / Published online: 5 July 2002

Abstract The Cangshang gold deposit of the north-western Jiaodong Peninsula contains reserves of greater than 50 tonnes (t) and is developed by the largest open pit gold mine in China. This deposit is a Jiaojia-style (i.e. disseminated-and-veinlet) deposit. It is controlled by the San-Cang fault zone, which trends ~040° and dips 40–75°SE at the mine site. The main (no. 1) orebody lies between a hanging wall of Precambrian metamorphic rocks (mainly amphibolite) of the Fenzishan Group and a footwall composed of the Mesozoic Linglong granitoid. The ore zone is mainly composed of pyritized, sericitized and silicified granitoid, which has undergone variable degrees of cataclasis. SHRIMP U–Pb dating of zircon indicates that the protolith of the hanging wall amphibolite was formed at 2530 ± 17 Ma and underwent metamorphism at 1852 ± 37 Ma. The footwall granodiorite has been dated at 166 ± 4 Ma, whereas zircons from the ore zone yield a younger age of 154 ± 5 Ma. Cathodoluminescence images of zircons from the granodiorite and ore zone show oscillatory zonation indicative of an igneous origin for both and the ages of these zircons, therefore, are all interpreted to be representative of magmatic crystallization. Dating of sericite by ^{40}Ar–^{39}Ar has been used to directly determine the timing of formation of the Cangshang deposit, providing the first time absolute age on formation of the Jiaojia-style gold deposits. The well-defined age of 121.3 ± 0.2 Ma provides the precise timing of gold mineralization at the Cangshang deposit. This age is consistent with those of Linglong-style (vein type) gold mineralization, also from the north-western Jiaodong Peninsula, at between 126 and 120 Ma. Therefore, our work indicates that both styles of gold deposits in the Jiaodong Peninsula were formed during the same mineralization event.

Keywords ^{40}Ar–^{39}Ar dating · Cangshang gold deposit · Gold mineralization · North China craton · SHRIMP U–Pb dating

Editorial handling: R. J. Goldfarb

X. Zhang (✉) · P.A. Cawood
Tectonics Special Research Centre,
School of Applied Geology, Curtin
University of Technology,
GPO Box U1987, Perth,
WA 6845, Australia
E-mail: zhang@lithos.curtin.edu.au
Tel.: +61-8-92663421
Fax: +61-8-92663153

X. Zhang · S.A. Wilde
School of Applied Geology,
Curtin University of Technology,
GPO Box U1987, Perth, WA 6845, Australia

R. Liu
Geological Academy, Ministry of Metallurgical Industry,
Tianjin City, 300061, P.R. China

H. Song · W. Li
Laizhou Gold Company, Shandong Province,
261440, P.R. China

L.W. Snee
United States Geological Survey, Box 25046,
MS 974, Denver Federal Center,
Denver, CO 80225-0046, USA

Introduction

Total gold reserves for China in 1998 were about 4,000 tonnes (t) with estimated potential resources of about 10,000 t (Zhou 1998). More than 3,000 gold deposits have been reported in various parts of China (Yang 1996), but they are predominantly distributed along the margins of the Precambrian cratons. Gold deposits in China are believed to have formed over a wide time period from early Palaeozoic to Cenozoic (Zhai and Deng 1996; Miller et al. 1998; Zhou et al. 2002), although much of this resource formed during the Yanshanian orogenic event (160–70 Ma), as the result of subduction of the Pacific plate under Eurasia (Zhai and Deng 1996). The Jiaodong Peninsula is situated along the south-eastern margin of the North China craton (inset of Fig. 1). This peninsula constitutes the most important gold province in China, with a number of lode-gold deposits combining to

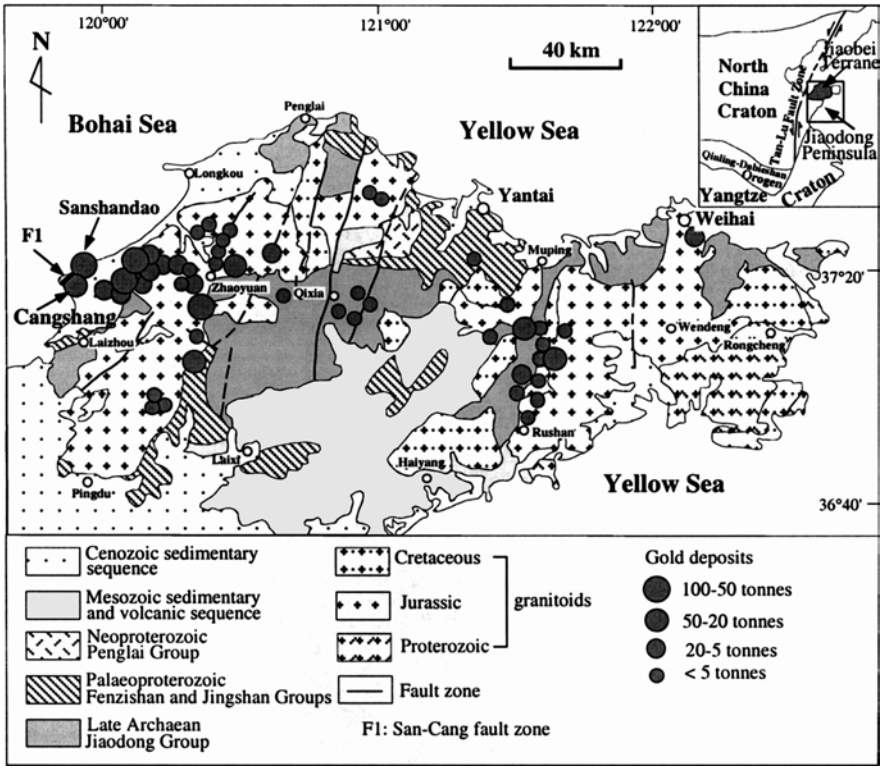

Fig. 1 Geological map of the northern Jiaodong Peninsula showing the distribution and size of gold deposits. *Inset map* indicates its location within the North China craton (modified from Shandong Bureau of Geology and Mineral Resources 1992)

contain 25% of China's total gold reserves (Zhou and Lü 2000; Zhou et al. 2002).

Jiaodong gold deposits are strongly controlled by fault zones (Liu 1987; Qiu et al. 2002), and are either of disseminated-and-veinlet type or of vein type. The former, which is locally termed Jiaojia-style, is associated with the regional NNE- to NE-trending fault zones, and is typically developed at lithologic contacts along the fault zones rather than within single rock units. These deposits occur where auriferous fluid infiltrates wall-rocks along the regional fault zones, and deposits quartz or sulphide veinlets and disseminated metal-bearing grains. Lode-gold deposits dominated by vein type are locally termed Linglong-style (Liu 1987). These deposits are controlled by secondary faults off the regional fault zones and occur where auriferous fluids filled large fractures developed in competent host rock. Qiu et al. (2002) inferred that both styles of gold deposit formed at the same time, based on the similarity of geological features, and also considered that they may be transitional parts of single deposits.

Of the two styles of mineralization, only the age of Linglong-style deposits has been well dated by both direct and indirect means. Yang and Zhou (2001) have recently obtained Rb–Sr isochron ages on pyrites of 123–122 Ma from the Linglong gold deposits. This is consistent with SHRIMP U–Pb zircon ages of the host rocks and post-mineralization dykes in the Linglong goldfield, which bracket the timing of this style of deposit between 126 and 120 Ma (Wang et al. 1998; Qiu et al. 2002). Whereas Wang et al. (1998) and Qiu et al. (2002) provided a maximum age (ca. 126 Ma) for the Jiaojia-style gold deposits, there has been no direct dating of this style deposit.

The Cangshang gold deposit (lat. 37°20′58.9″ to 37°21′44.0″N; long. 119°53′38″ to 119°54′51.2″E) lies about 20 km north of the city of Laizhou and is one of the largest deposits (reserves of 50–100 t) in the northwestern Jiaodong Peninsula (Fig. 1). The deposit is a typical Jiaojia-style gold occurrence. It is associated with the San-Cang fault zone, which also structurally controls the large Sanshandao gold deposit located 4 km north of Cangshang (Fig. 1). The Cangshang deposit is mined from the largest open pit in China, which exposes excellent geological features for research work.

This paper provides the first description of the geology and mineralization at the Cangshang gold deposit. More importantly, it provides both direct and indirect dates for the Jiaojia style deposits, based on ^{40}Ar–^{39}Ar age of sericites and SHRIMP U–Pb zircon ages of the host rocks.

Geological setting

The western boundary of the Jiaodong Peninsula is marked by the NNE-trending Tan-Lu fault zone (inset of Fig. 1). To the south, this peninsula is bounded by the Yangtze craton (inset of Fig. 1), although the precise location of its northern boundary is controversial (Okay and Sengör 1992; Yin and Nie 1993; Wang et al. 1998). Jiaodong gold deposits are located within the northern part of the Jiaodong Peninsula (Fig. 1), which is called the Jiaobei terrane (Qiu et al. 2002). This terrane represents a part of the basement of the North China craton. The Precambrian sequences of this terrane consist of the Late Archaean Jiaodong Group, the Palaeoproterozoic Fenzishan and Jingshan Groups, as well as the Neoproterozoic Penglai Group (Fig. 1), which are covered by

Mesozoic shales, clastic rocks and volcanic rocks (Zhou and Lü 2000). Mesozoic granitoid intrusions occupy about 43% of the surface area of the Jiaobei terrane (Qiu et al. 2002).

Wang et al (1998) identified two main phases of deformation within the Jiaobei terrane during the Mesozoic, with the first phase being NW–SE oblique compression, producing prominent NNE- to NE-trending brittle–ductile shear zones with sinistral oblique reverse movements. This was followed by reactivation involving development of brittle structures, which was accompanied by hydrothermal alteration and gold mineralization. The timing of the two phases of deformation is constrained between 165 and 120 Ma (Wang et al. 1998; Qiu et al 2002).

Cangshang gold deposit

The Cangshang gold deposit was discovered in 1984 by the No. 6 Team of Geology and Exploration, Bureau of Geology and Mineral Resources of the Shandong Province (BGMRSP), based on interpretation of geophysical data, 1:50,000 scale mapping and drilling. About 20,000 oz. of gold were produced in 1990, with the known reserves estimated at 28.724 t. By 2001, the known reserves were extended to 50 t, and 70,000 oz. of gold were produced in 2001, with an average grade of 4.81 g/t and daily ore production of 1,500 to 2,000 t (unpublished company data). In 2001, the Cangshang open pit was 850 m in length and 390 m in width. Mining depth was down to the minus-166-m bench, which is the designed final mining depth. A detailed map of the pit and the principal orebody (no. 1) is presented in Fig. 2.

The deposit is located at the contact between a hanging wall sequence of rocks of the Palaeoproterozoic Fenzishan Group to the south-east and the Mesozoic Linglong granitoid in the footwall to the north-west. The hanging-wall sequence was incorrectly considered to be part of the Late Archaean Jiaodong Group in the Chinese literature because of the lack of reliable geochronological data. The contact is marked by the San-Cangshang fault zone. This fault zone generally trends ~40° and dips 35–45°SE, and is poorly exposed on land and extends to the north-east and south-west into the Bohai Sea.

Deposit geology

Fenzishan Group

The Palaeoproterozoic Fenzishan Group (Fig. 2) makes up the hanging wall of the Cangshang gold deposit and, in the vicinity of the no. 1 orebody, comprises amphibolite, with lesser amounts of fine-grained gneiss and hornblendite. The amphibolite is fine-grained and consists of plagioclase and hornblende, with rare quartz and garnet. Accessory minerals include titanite, apatite and zircon. Where fresh, the unit has a grey-green to dark green colour. The amphibolite was metamorphosed to upper amphibolite facies. The fine-grained gneiss, which is intercalated with the amphibolite, is grey in colour and

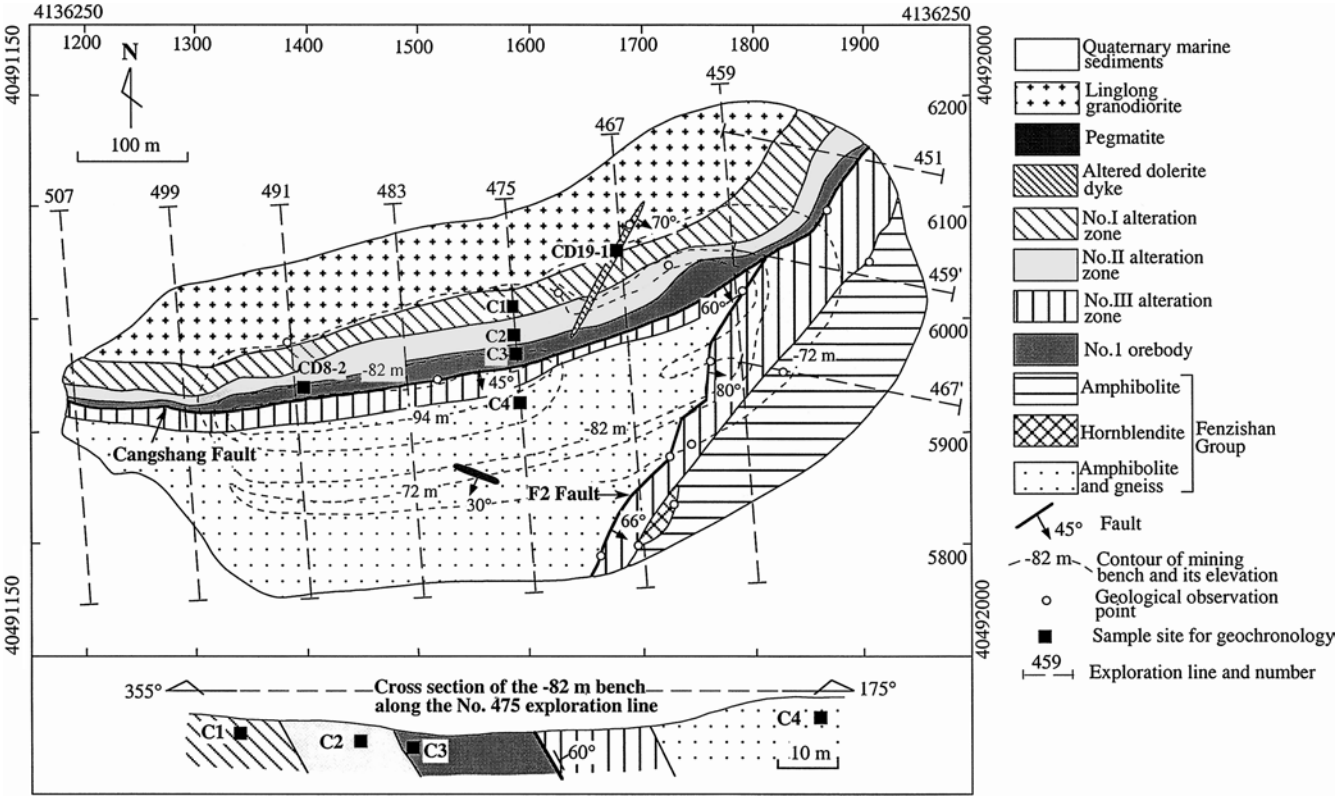

Fig. 2 Geologic map of the open pit of the Cangshang gold deposit showing the location of samples collected for geochronologic study

mainly composed of plagioclase, biotite and quartz. Accessory minerals include apatite and zircon. The hornblendite (>90% hornblende) is fine-grained, dark green in colour and has intruded the amphibolite.

Linglong Granitoid

The Linglong Granitoid (Fig. 2), which makes up the footwall of the Cangshang gold deposit, is exposed in the open pit and consists mainly of granodiorite, which is grey-white in colour and composed of plagioclase, quartz, K-feldspar and biotite. Accessory minerals include magnetite, allanite, apatite and zircon. It has a fine- to medium-grained, equigranular texture with a prominent foliation and is strongly fractured.

Late dykes

A series of pegmatite dykes (Fig. 2) occur in the pit and are flesh pink in colour and composed of K-feldspar, quartz and plagioclase, with minor biotite. They have a coarse-grained, massive structure and are unaltered, which suggests that they post-date gold mineralization.

An altered mafic dyke (Fig. 2) cuts the no. 1 orebody and the footwall granodiorite. It is yellow-green in colour, and has a porphyritic texture and massive structure. Because of strong alteration, its composition could not be precisely determined in the field. Microscopically, it consists of phenocrysts altered to chlorite, possibly after ferromagnesian minerals such as pyroxene and/or olivine; some tabular minerals in the groundmass were probably plagioclase, but are now altered to sericite. The dyke is inferred to be originally a dolerite. Based on field observations, the dyke post-dated gold formation, but its alteration indicates probable overlap with late hydrothermal stages.

Cangshang fault zone

The Cangshang fault zone is the south-western segment of the San-Cang fault zone. It is about 7 km long between the north-eastern (no. 203) and the south-western (no. 747) exploration lines (not shown on Fig. 2), and varies in width from 50 to 200 m. This fault zone has a general trend of ~040° and dips 40–75°SE. In detail, between the nos. 203 and 459′ exploration lines, it strikes 020° and dips 75°SE; between the nos. 459 and 563 exploration lines, it strikes 080–085° and dips 50°SE; and between the nos. 563 and 747 exploration lines, it strikes 045° and dips 40–50°SE. The sense of movement, deduced from the striations that plunge 45° towards 220°, is reverse and oblique. The fault zone is considered to be characteristic of compressional-shearing with dextral movement (No. 6 Team of Geology and Exploration, BGMRSP 1991). A main fault plane, marked by a grey-coloured fault gouge zone (10–20 cm in width), is present throughout the area.

Alteration

At the Cangshang deposit (Fig. 2), the alteration styles are dominantly silicification, sericitization, pyritization, K-feldspar alteration, chloritization and carbonation. A large alteration halo within the Cangshang gold deposit is well-developed along the Cangshang fault zone. Within the mining area, this alteration halo is 1,900 m in length, ranges from 85 to 185 m in width, and has been explored to a depth of 640 m. Based on the type and intensity of alteration and the nature and distribution of altered rocks, this alteration halo can be roughly divided into three subzones, although these change gradually and there are no clear boundaries between them. The alteration zones are the nos. I, II and III zones, respectively, on Fig. 2. The no. I alteration zone is situated below the main fault plane and adjacent to the footwall of Linglong granodiorite. This zone is characterized by K-feldspar alteration, sericitization and silicification and consists of altered Linglong granodiorite. The intensity of alteration is weaker than in the other zones, because it is farther away from the main fault plane. The no. II zone is developed below and adjacent to the main fault zone. This zone is characterized by strong pyrite alteration, sericitization and silicification and is composed mainly of pyrite–sericite–quartz rocks. The no. III alteration zone is located on the hanging wall side of the main fault plane, within and adjacent to rocks of the Fenzishan Group, but is terminated to the west by the F2 Fault, striking 015° and dipping 66–80°SE. This portion of the alteration zone is wider and extends for as much as 60 m into the hanging wall (Fig. 2). The no. III zone is characterized by sericitization, silicification and chloritization of the sheared rocks of the Fenzishan Group.

No. 1 orebody

The no. 1 orebody is predominantly controlled by the Cangshang fault zone (Fig. 2) and has 98% of the proven reserves. It lies within the no. II alteration zone and is as far as 50 m structurally below, and parallel to, the main fault plane (Fig. 2). The known length of the no. 1 orebody is 1,360 m between the nos. 449 and 547 exploration lines, and in the open pit the orebody is mainly exposed between the nos. 451 and 507 exploration lines (Fig. 2). The grade of the no. 1 orebody changes considerably throughout the deposit (see Fig. 3 for vertical changes in ore grade). Its average thickness is 9.98 m, with a maximum of 43.43 m; its mean grade is 4.81 g/t, with a maximum of 24.53 g/t. In the open pit, the no. 1 orebody mainly comprises pyritized, sericitized and silicified granitic rock, with different degrees of cataclasis. It lacks sharp boundaries within the no. II

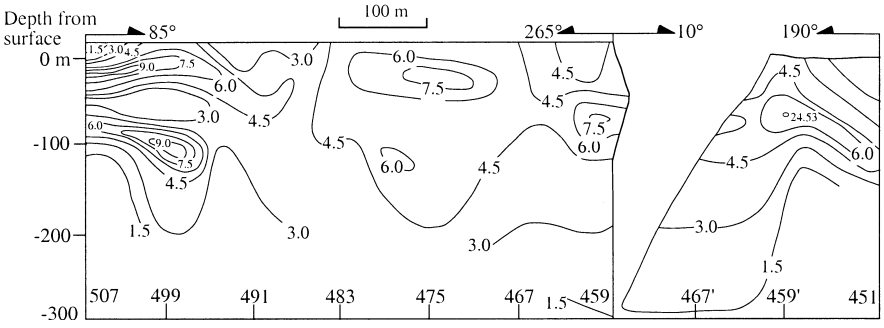

Fig. 3 Vertical section showing grade contours (in g/t Au) of the no. 1 orebody (the data are from the No. 6 Team of Geology and Exploration, BGMRSP 1991)

alteration zone and it is only distinguished by grade analysis with the cut-off taken at 2.13 g/t. The no. 1 orebody pitches in a north-easterly direction at 35–40°. To the north of the no. 459′ exploration line, the orebody strikes 021–050° and dips 70–88°SE; to the west of the no. 459 exploration line, it strikes 080–085° and dips 48–60°SE. The trend and sense of movement on the mineralized fault zone indicates that the orientation of maximum compression was approximately south-east–north-west. To the west of the no. 459 exploration line, there are two groups of mineralized fractures. The best developed set strike 070–090° and dip 40–60°SE, which is essentially concordant with the orebody. A second set strikes 040–060° and dips 50–70°SE (Fig. 4a). To the north of the no. 459′ exploration line, there only exists one set of mineralized fractures, which strike 040–050° and dip 45–65°SE (Fig. 4b; No. 6 Team of Geology and Exploration, BGMRSP 1991).

Ore mineralogy and paragenesis

Sulphide minerals in the deposit include mainly pyrite, sphalerite, galena, chalcopyrite and arsenopyrite. Among them, pyrite is the most abundant and the main gold-bearing mineral within the deposit. Gangue minerals dominantly comprise quartz, sericite, feldspar, calcite, barite and chlorite. Gold minerals are dominantly electrum with trace amounts of native gold. The ore consists mainly of quartz, sericite, pyrite and small amounts of other sulphide minerals, including sphalerite and galena. Based on the mineralogical, textural and crosscutting relationships observed in the field (Fig. 5), several stages of hydrothermal mineral formation have been identified. In total, four stages have been identified (Fig. 6) and, from the oldest to the youngest, these stages are stage 1 pyrite–quartz, stage 2 gold–quartz–pyrite, stage 3 quartz–base metal sulphide minerals and stage 4 quartz–calcite. Fluid inclusion studies suggest temperatures associated with stages 1 to 4 are 330–300, 300–250, 250–200 and 200–80 °C, respectively (No. 6 Team of Geology and Exploration, BGMRSP 1991).

The stage 1 mineral assemblage consists of coarse-grained pyrite and quartz, with minor arsenopyrite. The pyrite is light yellow-white in colour and has a strong metallic lustre. It generally forms euhedral cubes and ranges from 0.5 to 3.5 mm in diameter. Fractures are well-developed in the pyrite, and many other later stage sulphide minerals, such as chalcopyrite and galena, occur as infillings. The quartz is milk-white in colour, with a greasy lustre, and is coarse-grained with a subhedral habit.

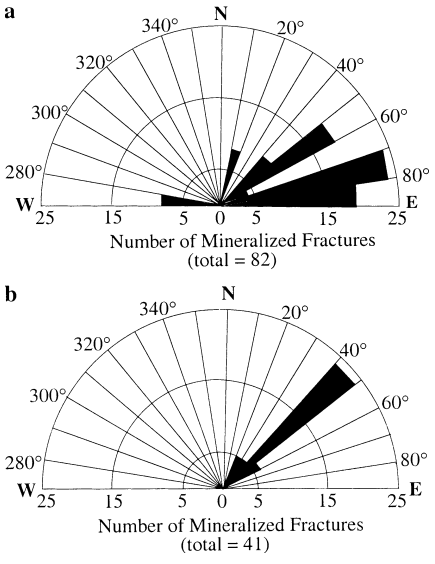

Fig. 4 Rose diagrams of orientations of mineralized fractures in the open pit of the Cangshang gold deposit **a** to the west of no. 459 exploration line, **b** to the east of no. 459 exploration line (based on data from the No. 6 Team of Geology and Exploration, BGMRSP 1991)

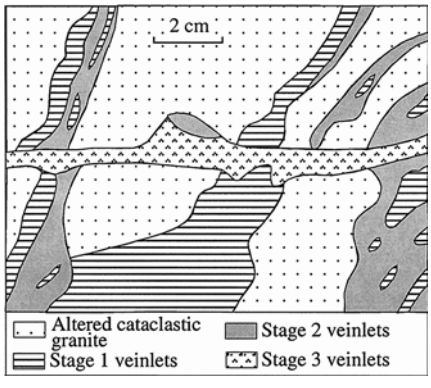

Fig. 5 A field sketch showing the crosscutting relationships amongst three stages of veining at the Cangshang gold deposit

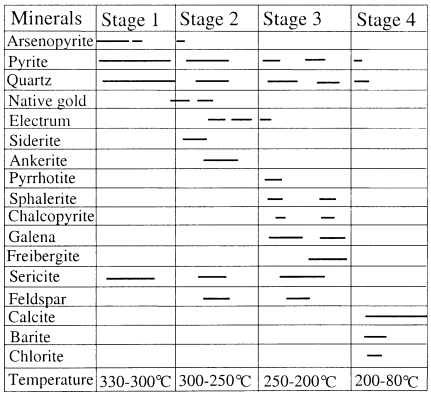

Fig. 6 Paragenetic sequence of hydrothermal minerals of the Cangshang gold deposit (data from the No. 6 Team of Geology and Exploration, BGMRSP 1991)

The mineral assemblage of stage 2 is dominantly pyrite, quartz, arsenopyrite, ankerite, siderite, electrum and native gold. The pyrite, light yellow in colour with a weak metallic lustre, generally forms euhedral cubes and is fine- to medium-grained (0.08–0.36 mm in diameter). The quartz is fine-grained and granular, with a light grey colour and vitreous lustre.

In stage 3, the mineral assemblage is more complex and dominantly composed of quartz, pyrite, chalcopyrite, galena, sphalerite and electrum. This paragenesis forms veinlet and disseminated mineralization. The dark yellow pyrite has a dull lustre and is very fine-grained (0.012–0.048 mm in diameter). The quartz is also very fine-grained, smoke-grey in colour, with a vitreous lustre.

The mineral assemblage in stage 4 mainly consists of calcite, quartz, barite and chlorite, occurring as veinlets filling late fractures. The calcite is typically anhedral with well-developed twins. Fine-grained subhedral quartz is distributed in the calcite aggregates. This stage post-dates the gold mineralization because it cuts the mineralized veins.

SHRIMP geochronological constraints

In order to provide constraints on the timing of gold mineralization, as well as to understand the geological evolution of the region, whole rock samples from the no. I alteration zone (C1), from the no. II alteration zone (C2), from the no. 1 orebody (C3) and from the hanging wall (C4) of the Cangshang gold deposit (Fig. 2) were selected for U–Pb zircon analysis. Unfortunately, sample C2 contained insufficient zircon for analysis. A sample from the altered dolerite dyke, which cuts the no. 1 orebody (CD19-1), was also processed. However, it lacked zircons, so the minimum age of the gold mineralization at the Cangshang gold deposit cannot be constrained in this manner.

Zircon analyses were carried out on a sensitive high resolution ion microprobe mass spectrometer (SHRIMP) operated at Curtin University of Technology. The SHRIMP analytical technique and data treatment are described in detail by Nelson (1997) and Williams (1998). SHRIMP results for the samples are listed in Table 1 and illustrated on concordia diagrams in Fig. 7. All errors for individual analyses in Table 1 are given as 1σ. Group ages in concordia plots are quoted with 95% confidence error limits (2σ).

Altered footwall granodiorite (sample C1)

Sample C1 from the no. I alteration zone of the Cangshang gold deposit (Fig. 2) is a weakly sericitized, medium-grained granodiorite with a hypido- to allotriomophic equigranular texture. It comprises plagioclase (50%), quartz (30%), potassic feldspar (18%), muscovite (2%), biotite (mostly replaced by muscovite, 1%), and minor calcite, apatite and zircon. Zircons are usually enclosed in quartz and range in colour from colourless to pale purple with most having a pale brown colour. The selected zircons vary in size from 74 to 132 μm and most are euhedral, with pyramidal terminations. The average elongation ratio is about 2:1, with a maximum of 4:1. Thirty-four analyses were made on 33 zircon grains (Table 1 and Fig. 7a), and ages range from 2542 ± 8 to 160 ± 7 Ma.

Ten analyses of the youngest ten grains from the sample form a coherent group (group 1 in Fig. 7a) with a weighted mean $^{206}Pb/^{238}U$ age of 166 ± 4 Ma and a chi-square value of 1.06. The U and Th contents of these ten spots range from 58 to 365 ppm and from 7 to 347 ppm, respectively (Table 1). The Th/U ratios vary from 0.06 to 1.00. Cathodoluminescence images of group 1 crystals indicate all are from grains with well-developed oscillatory zoning, which either constitutes the entire grain (Fig. 8a) or forms a broad rim surrounding a core (Fig. 8b). This growth pattern is indicative of crystallization from a melt (Vavra 1990) and the age of 166 ± 4 Ma is taken as the age of igneous crystallization of the footwall granodiorite.

The remaining zircons in the sample are considered to be inherited. These include a second relatively homogeneous group (group 2 in Fig. 7a) of six analyses of six zircons. The uranium content of spot 20.1 is very high (2,225 ppm), whereas the uranium contents of the other five spots range from 39 to 761 ppm. The thorium contents of the six spots range from 1 to 38 ppm, with Th/U ratios of 0.02 to 0.1 (Table 1). Cathodoluminescence imaging revealed group 2 analyses are all from oscillatory zoned zircons with some evidence of possible internal recrystallization (Fig. 8c). These give an age of 244 ± 11 Ma with a chi-square value of 2.41. This is coincident with the age of ca. 250–210 Ma for inherited zircons in the Linglong granitoid reported by Wang et al. (1998).

Inherited zircons occur with ages between 2200 and 800 Ma, but no statistical group could be defined (Fig. 7a). The oldest near-concordant $^{207}Pb/^{206}Pb$ age of

Table 1 SHRIMP U–Pb data for zircons from samples C1, C3 and C4 from the Cangshang gold deposit. Analyses are listed in order of increasing age. The following notation is used for analysed grains: *1.1* grain 1, first point analysed. Data are ^{204}Pb-corrected. Individual analyses have a 1σ error. The ^{206}Pb/^{238}U age is adopted for ages of less than 1.0 Ga, otherwise, the ^{207}Pb/^{206}Pb age is used

Spot	U (ppm)	Th (ppm)	Th/U	Total Pb (ppm)	$\frac{^{204}Pb}{^{206}Pb}$	$\frac{f206}{(\%)}$	$\frac{^{207}Pb}{^{206}Pb}$	$\frac{^{206}Pb}{^{238}U}$	$\frac{^{207}Pb}{^{235}U}$	$\frac{^{206}Pb}{^{238}U}$ Age	$\frac{^{207}Pb}{^{206}Pb}$ Age
Sample C1 (altered granodiorite)											
23.1	58	32	0.56	2	0.00762	0.122	0.027 ± 322	0.0251 ± 11	0.09 ± 11	160 ± 7	
15.1	104	92	0.89	3	0.00112	0.018	0.057 ± 148	0.0255 ± 7	0.20 ± 5	162 ± 5	
16.1	365	347	0.95	11	0.00000	0	0.054 ± 12	0.0257 ± 5	0.19 ± 1	163 ± 3	
9.1	138	100	0.72	4	0.00138	0.022	0.043 ± 97	0.0257 ± 7	0.15 ± 4	164 ± 4	
21.1	141	126	0.89	4	0.00167	0.027	0.037 ± 91	0.0258 ± 6	0.13 ± 3	164 ± 4	
11.1	119	41	0.34	3	0.00178	0.029	0.047 ± 114	0.0261 ± 7	0.17 ± 4	166 ± 4	
27.1	112	106	0.96	4	0.00138	0.022	0.048 ± 115	0.0263 ± 7	0.17 ± 4	167 ± 4	
5.1	95	95	1.00	3	0.00298	0.048	0.025 ± 44	0.0263 ± 8	0.09 ± 5	167 ± 5	
6.1	193	118	0.61	6	0.00042	0.007	0.051 ± 49	0.0267 ± 6	0.19 ± 2	170 ± 4	
2.1	119	7	0.06	3	0.00209	0.033	0.041 ± 107	0.0280 ± 7	0.16 ± 4	178 ± 5	
12.1	70	15	0.21	2	0.00061	0.01	0.064 ± 148	0.0285 ± 9	0.25 ± 6	181 ± 5	
7.1	469	641	1.37	17	0.00031	0.005	0.061 ± 30	0.0296 ± 6	0.25 ± 1	188 ± 4	
25.1	162	55	0.34	5	0.00085	0.014	0.048 ± 61	0.0319 ± 7	0.21 ± 3	202 ± 5	
26.1	761	18	0.02	26	0.00019	0.003	0.050 ± 15	0.0366 ± 7	0.25 ± 1	232 ± 5	
17.1	81	4	0.05	3	0.00099	0.016	0.047 ± 108	0.0381 ± 10	0.25 ± 6	241 ± 6	
13.1	99	10	0.10	4	0.00091	0.015	0.049 ± 77	0.0383 ± 10	0.26 ± 4	242 ± 6	
1.1	150	7	0.05	6	0.00041	0.007	0.051 ± 64	0.0398 ± 9	0.28 ± 4	251 ± 6	
20.1	2,225	38	0.02	81	0.00007	0.001	0.050 ± 6	0.0401 ± 8	0.28 ± 1	254 ± 5	
18.1	39	1	0.02	2	0.00210	0.034	0.048 ± 200	0.0403 ± 14	0.26 ± 11	254 ± 9	
33.1	230	163	0.71	16	0.00045	0.007	0.055 ± 27	0.0604 ± 13	0.45 ± 3	378 ± 8	
24.1	198	152	0.77	17	0.00050	0.008	0.060 ± 29	0.0683 ± 14	0.56 ± 3	426 ± 9	
29.1	131	81	0.62	13	0.00041	0.007	0.064 ± 28	0.0914 ± 20	0.81 ± 4	564 ± 12	
8.1	149	203	1.36	26	0.00054	0.009	0.062 ± 21	0.1330 ± 28	1.14 ± 5	805 ± 16	
28.1	552	235	0.43	143	0.00006	0.001	0.112 ± 5	0.2579 ± 51	3.97 ± 8		1,825 ± 9
4.1	562	246	0.44	213	0.00003	0	0.113 ± 4	0.3553 ± 70	5.52 ± 11		1,843 ± 7
4.2	591	123	0.21	211	0.00003	0	0.114 ± 4	0.3529 ± 70	5.55 ± 11		1,865 ± 7
32.1	907	167	0.18	326	0.00002	0	0.117 ± 3	0.3565 ± 70	5.74 ± 12		1,906 ± 5
14.1	170	57	0.34	66	0.00008	0.001	0.118 ± 10	0.3638 ± 75	5.93 ± 14		1,928 ± 15
22.1	704	108	0.15	261	0.00003	0	0.123 ± 4	0.3666 ± 73	6.20 ± 13		1,996 ± 7
31.1	270	73	0.27	95	0.00001	0	0.123 ± 7	0.3369 ± 68	5.71 ± 12		1,998 ± 10
19.1	233	65	0.28	92	0.00000	0	0.125 ± 7	0.3782 ± 76	6.53 ± 14		2,033 ± 10
30.1	283	160	0.56	125	0.00003	0	0.130 ± 7	0.3974 ± 80	7.12 ± 15		2,098 ± 9
3.1	76	75	0.99	36	0.00008	0.001	0.131 ± 15	0.4069 ± 88	7.32 ± 19		2,105 ± 20
10.1	204	144	0.70	120	0.00004	0.001	0.168 ± 8	0.4990 ± 101	11.58 ± 25		2,542 ± 8
Sample C3 (orebody)											
4.2	96	93	0.97	4	0.00246	0.173	0.072 ± 27	0.0227 ± 8	0.23 ± 9	145 ± 5	
2.1	137	49	0.36	4	0.00252	0.04	0.056 ± 12	0.0234 ± 5	0.18 ± 4	149 ± 3	
6.2	255	40	0.16	6	0.00182	0.022	0.056 ± 7	0.0239 ± 4	0.18 ± 2	152 ± 3	
5.1	1,060	168	0.16	25	0.00173	0.003	0.050 ± 2	0.0245 ± 3	0.17 ± 1	156 ± 2	
6.1	131	27	0.2	3	0.00018	0.007	0.075 ± 103	0.0245 ± 6	0.25 ± 4	156 ± 4	
4.1	85	91	1.06	3	0.00042	0.028	0.057 ± 14	0.0249 ± 6	0.19 ± 5	158 ± 4	
10.1	302	66	0.22	15	0.00137	0.022	0.059 ± 4	0.0462 ± 7	0.37 ± 2	291 ± 4	
1.1	41	26	0.61	5	0.00022	0.039	0.054 ± 10	0.0972 ± 21	0.72 ± 13	598 ± 13	
7.1	389	531	1.36	64	0.00048	0.004	0.066 ± 1	0.1271 ± 17	1.16 ± 2	771 ± 10	
3.1	112	63	0.56	22	0.00009	0.029	0.135 ± 5	0.1414 ± 23	2.62 ± 11		2,158 ± 61

Table 1 (Continued)

Spot	U (ppm)	Th (ppm)	Th/U	Total Pb (ppm)	$\frac{^{204}Pb}{^{206}Pb}$	$\frac{f206}{(\%)}$	$\frac{^{207}Pb}{^{206}Pb}$	$\frac{^{206}Pb}{^{238}U}$	$\frac{^{207}Pb}{^{235}U}$	$\frac{^{206}Pb}{^{238}U}$ Age	$\frac{^{207}Pb}{^{206}Pb}$ Age
8.1	77	55	0.72	34	0.01084	0.008	0.145 ± 2	0.3728 ± 56	7.47 ± 15		2,292 ± 21
9.1	187	55	0.29	95	0.00136	0.001	0.166 ± 8	0.4715 ± 64	10.79 ± 16		2,517 ± 8
Sample C4 (amphibolite)											
7.1	3	0	0.01	1	0.00677	0.108	0.077 ± 41	0.3348 ± 208	3.56 ± 195	1,125 ± 809	
2.1	5	1	0.23	2	0.00577	0.092	0.086 ± 27	0.3493 ± 162	4.14 ± 133	1,336 ± 638	
6.1	15	1	0.04	5	0.00133	0.021	0.110 ± 7	0.3368 ± 85	5.1 ± 38	1,796 ± 123	
14.1	4	0	0.01	1	0.00321	0.051	0.110 ± 23	0.3319 ± 144	5.04 ± 111	1,801 ± 393	
27.1	44	1	0.02	14	0.00117	0.019	0.111 ± 5	0.3175 ± 64	4.86 ± 24	1,815 ± 76	
3.1	54	1	0.02	18	0.00026	0.004	0.114 ± 2	0.3357 ± 64	5.28 ± 16	1,865 ± 37	
16.1	15	0	0.02	5	0.00184	0.03	0.114 ± 9	0.3334 ± 86	5.25 ± 46	1,868 ± 145	
13.1	88	14	0.16	30	0.00008	0.001	0.121 ± 2	0.3413 ± 61	5.71 ± 13	1,975 ± 22	
15.1	3	0	0.04	1	0.00571	0.091	0.124 ± 33	0.3477 ± 187	5.94 ± 166	2,013 ± 491	
23.1	5	3	0.48	3	0.00509	0.081	0.127 ± 32	0.3229 ± 166	5.63 ± 147	2,050 ± 453	
8.1	4	1	0.12	2	0.00472	0.075	0.134 ± 25	0.3838 ± 176	7.06 ± 142	2,144 ± 339	
20.1	16	1	0.04	9	0.00869	0.139	0.134 ± 17	0.36 ± 111	6.64 ± 89	2,147 ± 222	
22.1	50	5	0.11	20	0.00099	0.016	0.134 ± 4	0.3721 ± 71	6.88 ± 24	2,151 ± 48	
26.1	67	30	0.45	31	0.00141	0.022	0.142 ± 4	0.39 ± 75	7.61 ± 29	2,246 ± 53	
10.1	2	0	0.01	2	0.00269	0.043	0.148 ± 25	0.4655 ± 264	9.49 ± 175	2,321 ± 293	
1.1	670	226	0.34	307	0.00003	0	0.154 ± 4	0.426 ± 71	9.04 ± 16	2,391 ± 5	
9.1	358	159	0.44	171	0.00009	0.001	0.158 ± 1	0.4317 ± 73	9.42 ± 17	2,437 ± 7	
18.1	58	10	0.17	34	0.00086	0.014	0.158 ± 3	0.5235 ± 99	11.43 ± 30	2,438 ± 26	
4.1	96	26	0.27	49	0.00015	0.002	0.159 ± 1	0.4785 ± 86	10.46 ± 22	2,440 ± 14	
17.1	10	1	0.12	4	0.00429	0.069	0.161 ± 20	0.3412 ± 140	7.59 ± 104	2,470 ± 215	
24.1	41	16	0.39	21	0.00061	0.01	0.163 ± 4	0.4456 ± 89	9.99 ± 33	2,482 ± 40	
12.1	42	15	0.36	23	0.00039	0.006	0.163 ± 2	0.4912 ± 96	11.05 ± 28	2,488 ± 24	
5.1	36	10	0.28	18	0.00043	0.007	0.166 ± 3	0.4632 ± 92	10.61 ± 29	2,518 ± 28	
21.1	186	175	0.94	115	0.00021	0.003	0.167 ± 1	0.491 ± 77	11.3 ± 20	2,528 ± 10	
11.1	83	37	0.44	43	0.00023	0.004	0.167 ± 1	0.4632 ± 82	10.67 ± 22	2,528 ± 14	
25.1	186	149	0.8	102	0.00011	0.002	0.168 ± 1	0.4554 ± 72	10.57 ± 19	2,541 ± 12	
19.1	94	42	0.44	51	0.00028	0.005	0.170 ± 2	0.4783 ± 80	11.18 ± 23	2,553 ± 17	

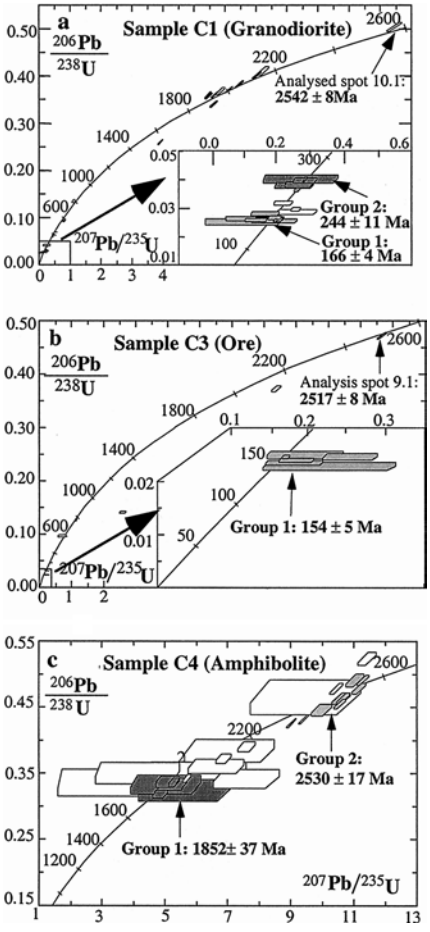

Fig. 7 U–Pb concordia diagrams showing total SHRIMP data for **a** sample C1 (host rock of weakly altered granodiorite), **b** sample C3 (orebody) and **c** sample C4 (host rock of amphibolite) from the Cangshang gold deposit. Error boxes are 1σ

2542 ± 8 Ma (1σ) was obtained from an inherited core (spot 10.1 in Fig. 7a).

Orebody (sample C3)

Sample C3 was taken from a strongly altered granitic cataclasite within the no. 1 orebody of the Cangshang Gold Deposit (Fig. 2). The rock has undergone extensive silicification, along with pyrite and sericite alteration. The rock is now composed mainly of quartz (80%), sericite (18%) and opaque minerals (2%). The zircons are contained mainly in sericite aggregates and also within quartz. The zircons analysed range in size from 105 μm to minus 74-μm and are colourless. They vary in shape from rounded to euhedral and the average elongation ratio is about 2:1. Twelve analyses were carried out on ten zircon grains, with ages ranging from 2517 ± 8 to 145 ± 5 Ma (Table 1 and Fig. 7b).

The main population consists of six analyses of four grains, which form a coherent group (group 1 in Fig. 7b) and have a weighted mean $^{206}Pb/^{238}U$ age of 154 ± 5 Ma with a chi-square value of 1.59. The uranium content of spot 5.1 is high (1,060 ppm), whereas the uranium contents of the other five spots range from 85 to 302 ppm. The thorium contents of the six spots range from 27 to 168 ppm, with Th/U ratios of 0.2 to 1.06 (Table 1). Cathodoluminescence images show oscillatory zonation patterns (Fig. 8d), which suggests that these grains are magmatic in origin and 154 ± 5 Ma is interpreted as the age of the host to the orebody. The age of 154 ± 5 Ma may represent either a slightly later period of granite crystallization, or a granitic dyke emplaced along the eventual ore zone after intrusion of the footwall granodiorite at 166 ± 4 Ma. It thus provides the maximum age of gold-related alteration at the Cangshang gold deposit.

Analysis spot 9.1 yields the oldest inherited concordant $^{207}Pb/^{206}Pb$ age of 2517 ± 8 Ma (1σ; Fig. 7b), which coincides with the oldest inherited zircon age

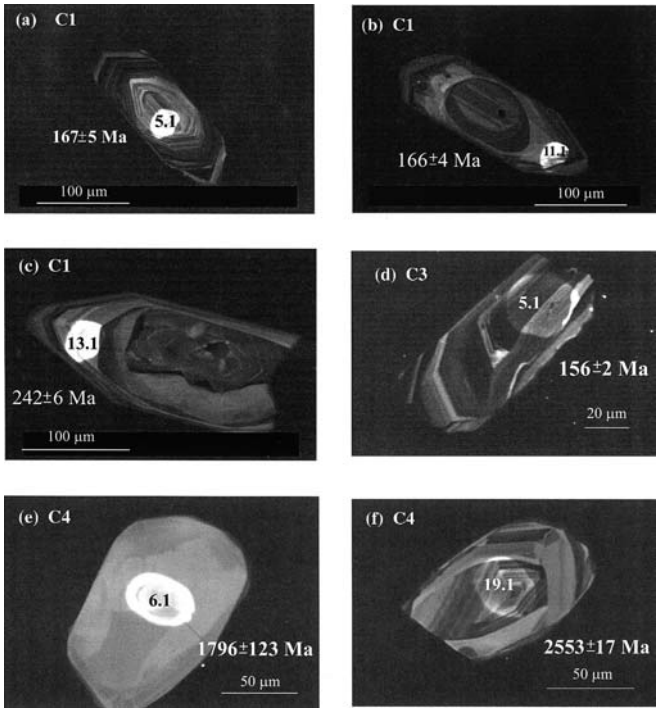

Fig. 8a–f A selection of cathodoluminescence (CL) images of zircons extracted from samples C1, C3, and C4 from the Cangshang gold deposit. *Scales* are given on photographs in μm. The *white circles* are the SHRIMP ion-probe analysis spots. **a** Zircon grain 5 of sample C1, showing the very distinct magmatic oscillatory zonation throughout the crystal. The $^{206}Pb/^{238}U$ age of spot 5.1 is 167 ± 5 Ma. **b** Zircon grain 11 of sample C1, showing a distinct core overgrown by a younger rim. The $^{206}Pb/^{238}U$ age of spot 11.1 is 166 ± 4 Ma. **c** Zircon grain 13 of sample C1, showing oscillatory zonation with some evidence of possible internal recrystallization. Spot 13.1 is located in the oscillatory zoned portion and its $^{206}Pb/^{238}U$ age is 242 ± 6 Ma. **d** Zircon grain 5 of sample C3, showing igneous oscillatory growth zones. The $^{206}Pb/^{238}U$ age of spot 5.1 is 156 ± 2 Ma. **e** Zircon grain 6 of sample C4 showing no structural zoning and a bright CL pattern. The $^{207}Pb/^{206}Pb$ age of spot 6.1 is 1796 ± 123 Ma. **f** Zircon grain 19 of sample C4 shows concentric growth zoning, which is typical of magmatic zircons, and a bright low-uranium content of the metamorphic rim. The $^{207}Pb/^{206}Pb$ age of spot 19.1 is 2553 ± 17 Ma

(2542 ± 8 Ma) of sample C1. Accordingly, the age of ca. 2500 Ma represents a Late Archaean igneous event in the basement of this region.

Hanging-wall amphibolite (sample C4)

Sample C4 was obtained from the hanging wall of the no. 1 orebody of the Cangshang gold deposit (Fig. 2) and is an amphibolite containing green and brown hornblende (48%), plagioclase (40%) and pyroxene (10%), as well as accessory grains of quartz. Zircons occur within the hornblende and those analysed range in size from plus 132 to minus 74-μm. They are pale purple to colourless, and neither optical zoning nor cores are evident. Twenty-seven analyses were undertaken on 27 zircon grains, and ages vary from 2553 ± 17 to 1125 ± 809 Ma (Table 1).

Six analyses of six zircons define a concordant population (group 1 in Fig. 7c) with a $^{207}Pb/^{206}Pb$ age of 1852 ± 37 Ma. Another zircon population consists of seven analyses of seven zircons, which form a cluster of variously discordant analyses (group 2 in Fig. 7c) having a weighted mean $^{207}Pb/^{206}Pb$ age of 2530 ± 17 Ma.

Under Cathodoluminescence, the two different populations of zircons (groups 1 and 2) exhibit distinct patterns. The younger zircon portions (group 1) luminesce brightly, indicating low uranium content, and have no structural zoning (Fig. 8e). The older zircons (group 2) have well-defined concentric growth zoning, which is typical of magmatic zircons, and have low-uranium (bright) overgrowths (Fig. 8f). This evidence substantiates that the older zircon represents the age of the igneous protolith and that the younger zircon formed during a major metamorphic event resulting in metamorphic overgrowth of zircon rims onto pre-existing zircons and also the formation of new grains (Fig. 8e).

^{40}Ar–^{39}Ar geochronology

Because white mica is a common hydrothermal mineral in these gold deposits, ^{40}Ar–^{39}Ar dating of this mica is a potentially useful technique for determining the timing of gold mineralization. This is particularly so in regions where ambient temperatures during mineralization were below the closure temperature (350 ± 50 °C) for argon diffusion in muscovite (McDougall and Harrison 1988), which is the case here (see Fig. 6). Muscovite is also resistant to diffusive argon loss when subjected to post-crystallization thermal disturbances (Dunlap et al. 1991) and rarely incorporates large amounts of excess ^{40}Ar (McDougall and Harrison 1988).

Strict definitions of age plateaus, which assume volume diffusive behaviour during vacuum heating, have not been used for hydrous minerals such as muscovite, as they degas largely by dehydroxylation and other mechanisms (Hodges et al. 1994), rather than by volume diffusion. Instead, using the age of plateau-like segments (i.e. flat portions in ^{40}Ar–^{39}Ar spectra) has been advocated (Kent and Hagemann 1996). Ages of plateau-like segments can be calculated by weighing the age and precision of each step to the amount of ^{39}Ar released. If steps are older or younger than the majority of steps in the plateau-like segment, they are not included in the final age calculation.

Based on the above assumptions and in order to better constrain the age of gold mineralization at the Cangshang gold deposit, hydrothermal muscovite from sample CD8-2 (Fig. 2) from the no. 1 orebody was selected for analysis by the ^{40}Ar–^{39}Ar technique. In hand specimen, sample CD8-2 is green-grey in colour and consists of quartz, muscovite and opaque minerals. Muscovite commonly occurs as aggregate among quartz grains. In thin section, the size of individual muscovite flakes ranges from 20 to 800 μm, but is generally in the range of 150–350 μm. These flakes surround quartz and opaque minerals. Quartz is common and shows undulose extinction. Auriferous pyrite occurs in textural equilibrium with muscovite as euhedral crystals. The muscovite separate was prepared using standard heavy-liquid techniques (Kent and McDougall 1995). A 79.3-mg separate with high purity was sent to the US Geological Survey's isotope laboratories in Denver, Colorado, for argon analysis. A detailed description of the ^{40}Ar–^{39}Ar analytical technique used in the Denver laboratories may be found in Shaw et al. (1999).

The ^{40}Ar–^{39}Ar release data are presented in Table 2 and age spectrum and isochron diagrams for sample CD8-2 are shown in Fig. 9. Errors for apparent ages in Table 2 are given as 1σ. The plateau-like segment age and corresponding isochron age in Fig. 9 are quoted with 95% confidence error limits (2σ). In this study, 12 temperature steps were used. The ^{40}Ar–^{39}Ar spectrum of muscovite (Fig. 9a) from sample CD8-2 exhibits young ages in the early stages (steps 1, 2 and 3) and final stage (step 12) of gas release, and illustrates well-defined plateau-like segments (steps 4–11) with 95.6% of ^{39}Ar released corresponding to an age of 121.3 ± 0.2 Ma. The isochron age is 121.1 ± 0.5 Ma (Fig. 9b), which is identical within error to the age of the plateau-like segments. Because the age spectrum for sample CD8-2 reveals no indication of argon loss sufficient to significantly lower the plateau-like segment age, the ^{40}Ar–^{39}Ar age of ca. 121 Ma obtained from muscovites is interpreted as the time of gold mineralization at the Cangshang deposit.

Discussion

The Cangshang gold deposit is a structurally controlled ore system within the local Cangshang fault zone and is associated with a zone of auriferous alteration as wide as 185 m. The Cangshang fault zone underwent several deformational episodes, with the trend and sense of movement on the mineralized fault zone indicating that the orientation of maximum compression was approximately south-east–north-west during the period of gold

Table 2 ^{40}Ar–^{39}Ar release data for sericite separates from the sample CD8-2 from the Cangshang gold deposit

Temp. (°C)	Radiogenic ^{40}Ar (10^{-16} mol)	K-derived ^{39}Ar (10^{-13} mol)	F Value	Radiogenic yield	^{39}Ar (%)	Apparent age (Ma at 1σ)
500	0.31573	0.02601	12.137	56.1	1.0	105.07 ± 1.06
600	0.21375	0.01619	13.199	87.8	0.6	113.97 ± 1.55
700	0.83953	0.06106	13.749	94.3	2.4	118.57 ± 0.33
800	2.86703	0.20208	14.188	97.2	7.8	122.23 ± 0.18
850	2.99296	0.21271	14.070	97.6	8.2	121.25 ± 0.18
900	3.85203	0.27404	14.057	97.5	10.6	121.13 ± 0.18
950	5.79932	0.41441	13.994	98.2	16.1	120.62 ± 0.18
1,000	7.39248	0.52588	14.057	98.9	20.4	121.14 ± 0.29
1,050	7.42284	0.52608	14.110	98.7	20.4	121.58 ± 0.23
1,100	3.22358	0.22886	14.085	98.1	8.9	121.37 ± 0.18
1,150	1.17392	0.08347	14.063	96.7	3.2	121.19 ± 0.44
1,250	0.14430	0.01049	13.750	88.0	0.4	118.58 ± 2.28

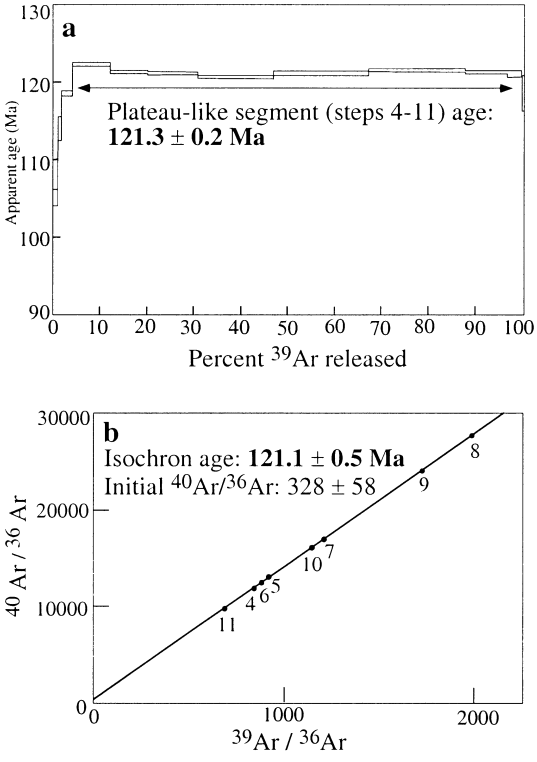

Fig. 9a, b Age spectrum for hydrothermal muscovites from sample CD8-2 from the Cangshang gold deposit. **b** Isochron diagram of plateau-like segments (steps 4–11) in **a**

mineralization. It forms part of a larger structure, the San-Cang fault zone, which is a deep, ductile shear zone with superimposed later brittle components that probably ultimately relate to the Eurasian and Pacific plate interactions during the late Mesozoic. The nearby first-order Tan-Lu fault zone, which constitutes a major lithospheric fracture, has been proposed as a fluid pathway for mineralization in the Jiaobei terrane (Zhang 1990; Cai 1993; Ren et al. 1997) and may have been the main regional fluid conduit.

The Cangshang gold deposit is a Jiaojia-style (i.e. disseminated-and-veinlet) gold deposit. It is situated at the contact between a hanging-wall sequence of Palaeoproterozoic Fenzishan Group amphibolite and a footwall sequence of Mesozoic Linglong granitoid. The alteration styles at the Cangshang gold deposit include silicification, sericitization, pyritization and K-feldspar alteration, which are consistent with other gold deposits in the Jiaobei terrane (Wang et al. 1998). On the basis of the mineralogical, textural and crosscutting relationships, four stages of veining have been identified, consisting of pyrite–quartz (stage 1), gold–quartz–pyrite (stage 2), quartz–base metal sulphide (stage 3) and quartz–calcite (stage 4). During stages 2 and 3, disseminated-and-veinlet style gold deposition formed the main orebodies.

The host rock in the footwall of the no. 1 ore zone is granodiorite with a crystallization age of 166 ± 4 Ma, obtained from whole zircon grains and zircon overgrowths. The no. 1 ore zone mainly consists of pyritized, sericitized and silicified granitic rock with different degrees of cataclasis. The zircons obtained from it have an age of 154 ± 5 Ma and cathodoluminescence images reveal oscillatory zoning, suggestive of a magmatic origin. Therefore, the host granitoid was crystallized at ca. 166–154 Ma. It belongs to the Linglong granitoid suite (with ages between 165 and 150 Ma) of Wang et al. (1998), which is related to the Yanshanian tectono-magmatic event (Xu et al. 1989). The age of 154 ± 5 Ma could be interpreted to indicate the age of one magmatic episode within the Yanshanian orogen. During this stage, a younger granitoid possibly intruded along the contact between the granodiorite (166 ± 4 Ma) and amphibolite (1852 ± 37 Ma) and was strongly altered and deformed during ore formation. Accordingly, this provides a maximum age for gold mineralization at the Cangshang gold deposit. However, the host granodiorite of the Sanshandao gold deposit, also controlled by the San-Cang fault zone, is 128 ± 2 Ma (Wang et al. 1998) and these two deposits have essentially the same ore minerals and alteration assemblages (Qiu et al. 2002). Therefore, it can be argued that the age of 128 ± 2 Ma indirectly constrains the maximum age of gold mineralization event in this area.

In order to directly determine the timing of formation of the Cangshang gold deposit, Ar–Ar dating of sericite

from the gold orebody was carried out. The well-defined plateau-like segment age of 121.3 ± 0.2 Ma provides the precise time of Cangshang deposit formation. In a recent study, Yang and Zhou (2001), using the Rb–Sr method on pyrite in gold-bearing quartz veins, directly dated the age of formation of the Linglong gold deposit (Linglong-style) in the north-western Jiaodong Peninsula as 123-122 Ma. In addition, the ages of the host rocks and a post-mineralization porphyry dyke in the Linglong goldfield, determined by the SHRIMP zircon U–Pb technique, constrained the age of gold mineralization at between 126 and 120 Ma (Wang et al. 1998; Qiu et al. 2002). Therefore, the sericite Ar–Ar age for the formation of the Jiaojia-style gold deposit at Cangshang is consistent with the age of Linglong-style gold deposits in the north-western Jiaodong Peninsula. Furthermore, our results confirm that there was a single lode-gold mineralization event (ca. 123–121 Ma) in the north-western Jiaodong Peninsula (Wang et al. 1998) during which both Jiaojia-style and Linglong-style gold deposits were formed.

Miller et al. (1998) pointed out that multiple orogenic events and associated magmatic activity, along with crustal scale structures at terrane and craton sutures, provide a favourable metallogenic scenario for gold deposits along the margins of the North China craton. The Jiaobei terrane of the Jiaodong Peninsula, which is located along the south-eastern border of the North China craton, experienced both strong Indosinian (early Mesozoic) and Yanshanian (late Mesozoic) orogenies (Wang et al. 1998). Therefore, its unique tectonic setting, leading to a very favourable system of fluid conduits, may explain why such large gold deposits occur in this area. Wang et al. (1998) showed that the geological and isotopic characteristics of the gold deposits in the Jiaodong region are consistent with derivation of the ore fluid from deep-seated sources in the lower crust and/or mantle.

Acknowledgements The authors thank A. Nemchin for beneficial discussions and kind assistance with SHRIMP analysis. P.D. Kinny and G.C. Zhao are also thanked for their helpful discussions, and we are particularly grateful to B. Cikara for patient assistance with zircon preparation. We thank two reviewers – Drs R.J. Goldfarb and Y.M. Qiu – for their critical comments and helpful suggestions that led to substantial improvements to the manuscript. The research reported here was supported by a grant to S.A. Wilde and P.A. Cawood from the Western Australia/China Economic and Technical Research Fund. Fieldwork was supported by the National Natural Science Foundation of China and the Laizhou Gold Company, Shandong Province, P.R. China. Tectonics Special Research Publication no. 181.

References

Cai XP (1993) Significance of the Tanlu fault zone on forming the concentrated area of gold deposits in the Jiaodong region (in Chinese with English abstract). Shandong Geol 9(2):93–101

Dunlap JD, Teyssier C, McDougall I, Baldwin S (1991) Ages of deformation from K/Ar and $^{40}Ar/^{39}Ar$ dating of white mica. Geology 19:1213–1216

Hodges KV, Hames WE, Bowring SA (1994) $^{40}Ar/^{39}Ar$ gradients in micas from high temperature–low-pressure metamorphic terrain: evidence for very slow cooling and implications for the interpretation of age spectra. Geology 22:55–58

Kent AJR, Hagemann SG (1996) Constraints on the timing of lode-gold mineralization in the Wiluna greenstone belt, Yilgarn Craton, Western Australia. Aust J Earth Sci 43:573–588

Kent, AJR, McDougall I (1995) $^{40}Ar/^{39}Ar$ and U–Pb Age constraints on the timing of gold mineralization in the Kalgoorlie Gold Field, Western Australia. Econ Geol 50:845–859

Liu LD (1987) Genesis of the most important lode-gold deposits in China (in Chinese with English Abstract). J Changchun Inst Geol 17(4):373–382

McDougall I, Harrison TM (1988) Geochronology and thermochronology by the $^{40}Ar/^{39}Ar$ method. Oxford University Press, Oxford

Miller LD, Goldfarb RJ, Nie FJ, Hart CJR, Miller ML, Yang YQ, Liu YQ (1998) North China Gold: a product of multiple orogens. Soc Econ Geol Newsl 33:6–12

Nelson DR (1997) Compilation of SHRIMP U–Pb zircon geochronological data, 1996. Geological Survey of Western Australia, Record 1997/2

No. 6 Team of Geology and Exploration, BGMRSP (1991) Geology Report of the Cangshang gold deposit (in Chinese), unpublished

Okay AI, Sengör AMC (1992) Evidence for continental thrust-related exhumation of the ultra-high-pressure rocks in China. Geology 20:411–414

Qiu YM, Groves DI, McNaughton NJ, Wang L, Zhou T (2002) Nature, age and tectonic setting of orogenic lode-gold mineralization in the Jiaodong Peninsula of North China Craton, China. Miner Deposita 37:283–305 DOI 10.1007/s00126-001-0238-3

Ren YS, Lin G, Peng XL (1997) Control of the Tanlu fault system on gold deposits in the western Jiaodong region (in Chinese with English abstract). Gold 18(2):3–7

Shandong Bureau of Geology and Mineral Resources (1992) Geological outline of gold deposits in the Shandong Province (in Chinese), unpublished

Shaw CA, Snee LW, Selverstone J, Reed JC Jr (1999) $^{40}Ar/^{39}Ar$ thermochronology of Mesoproterozoic metamorphism in the Colorado Front Range. J Geol 107:49–67

Vavra G (1990) On the kinematics of zircon growth and its petrogenetic significance: a cathodoluminescence study. Contrib Mineral Petrol 106:90–99

Wang LG, Qiu YM, McNaughton NJ, Groves DI, Luo ZK, Huang JZ, Miao LC, Liu YK (1998) Constraints on crustal evolution and gold metallogeny in the Northwestern Jiaodong Peninsula, China, from SHRIMP U–Pb zircon studies of granitoids. Ore Geol Rev 13:275–291

Williams IS (1998) U–Th–Pb geochronology by ion microprobe. In: Mckibben MA, Shanks WC III, Ridley W (eds) Applications of microanalytical techniques to understanding mineralizing processes. Econ Geol 7 (in press)

Xu JF, Shen BY, Niu LZ, Zheng WS (1989) Research on the granitoids related to gold mineralization in the Jiaobei terrane (in Chinese with English abstract). Shandong Geol 5(2): 1–125

Yang JH, Zhou XH (2001) Rb–Sr, Sm–Nd, and Pb isotope systematics of pyrite: implications for the age and genesis of lode gold deposits. Geology 29:711–714

Yang KH (1996) Gold deposits in China: main types and potential. Int Geol Rev 38:1006–1019

Yin A, Nie S (1993) An indentation model for the North and South China collision and the development of the Tan-Lu and Honam fault systems, eastern Asia. Tectonics 12:801–813

Zhai Y, Deng J (1996) Outline of the mineral resources of China and their tectonic setting. Aust J Earth Sci 43:673–685

Zhang ZM (1990) The forming condition and the distributive pattern of hydrothermal gold deposits in the Jiaobei Uplift (in Chinese). J Geol Explor 4:13–16

Zhou TH (1998) Major gold provinces and tectonics of China. Geol Soc Aust, Abstr no 49

Zhou TH, Goldfarb RJ, Phillips GN (2002) Tectonics and distribution of gold deposits in China – an overview. Miner Deposita 37:249–282 DOI 10.1007/s00126-001-237-4

Zhou TH, Lü GX (2000) Tectonics, granitoids and Mesozoic gold deposits in East Shandong, China. Ore Geol Rev 16:71–90